Spatiotemporal Brain Imaging: Microscopic&Systems Level (EB00790-05).

Overall goals and objectives

Our overall goal is to improve the spatial and temporal resolution of non-invasive technologies (such as fMRI or MEG/EEG), so that they can resolve more discrete (e.g., column and laminar level) neural units which bridge the systems and cellular levels; and to clarify the mechanisms which relate the biophysics of neuronal activity to "observables" in our imaging measurements (Fig. 1).

To achieve this goal, we develop an integrated suite of technologies capable of sufficient sensitivity to the observable physiological and biophysical parameters, with high spatial and temporal resolution to measure direct and indirect consequences of brain neuronal activity. We then use the developed tools to relate macroscopic measures to the underlying biophysics and cellular organization of the brain at the microscopic scale. Specifically, we consider multiple physiological processes, from macroscopic hemodynamic changes to the microscopic neurovascular communication and neuronal network behavior. Our approach is to address individual stages/relationships at the appropriate scale, with measures that directly reflect the parameters of interest. To bridge individual stages we define "transfer functions" between parameters in an integrated model that describes macroscopic observables in terms of underlying processes of vascular and neuronal activity.

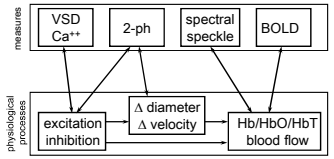

Figure 1. Conceptual framework for integration of measurement modalities.

The relationship between the measurements (voltage-sensitive (VSD) and calcium-sensitive (Ca^{++}) neuronal imaging, 2-photon laser scanning microscopy (2-ph), spectral imaging of intrinsic signals (spectral), laser speckle imaging of blood flow (speckle) and BOLD fMRI (BOLD)), and the physiological processes they measure (neuronal excitation and inhibition, microscopic changes in vascular diameter and blood flow velocity, and macroscopic changes in blood oxygenation and flow).

From neuronal excitation/inhibition to "positive" and "negative" hemodynamic response.

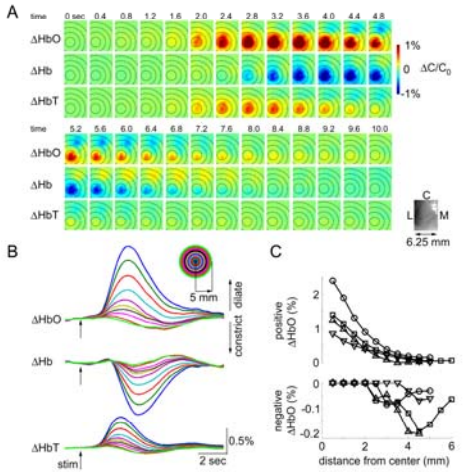

Figure 2. Spectroscopic optical imaging of blood oxygenation.

All three spectroscopic measures (oxy- deoxy- and total hemoglobin (HbO, Hb and HbT)) showed an antagonistic center-surround activation pattern where the central area of the response was surrounded by an area of the opposite sign. ***A***, ΔHbO, ΔHb and ΔHbT in response to a somatosensory (forepaw) stimulus. Time (in seconds) relative to stimulus onset (t=0) is indicated above images. The time series from the upper panel continues on the lower panel. The color-scale is expressed in percent change from the baseline ($\Delta C/C_0$). An image of raw vasculature corresponding to functional frames is shown in lower left corner. L – lateral, M – medial, C – caudal. ***B***, Signal time-courses extracted from 0.5 mm concentric rings around the center of the response. The center was estimated using the earliest HbT response. The rings are superimposed on images in *A*. Every other ring is shown. The inset shows the color code. ***C***, Peak positive (upper panel) and peak negative (lower panel) HbO signal change as a function of distance from the center. Data from 4 animals are superimposed (circles, squares, upward triangles, downward triangles).

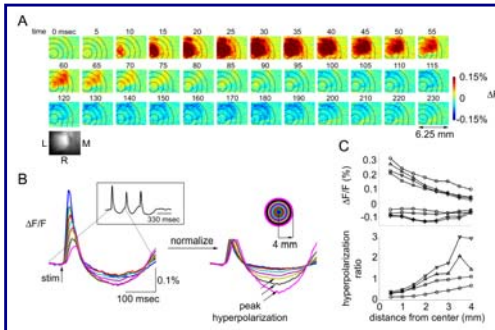

Figure 3. Imaging of 'surround" inhibition with voltage-sensitive dyes (VSD).

Comparison of the hyperpolarization ratio (the ratio of peak hyperpolarization to peak depolarization) to the hemodynamic data (Fig. 2) within the same range of distances reveals a correlation of negative hemodynamic signals (evoked decrease in blood oxygenation and volume) with relative hyperpolarization (neuronal inhibition). ***A***, VSD signal in response to the forepaw stimulus. Time relative to stimulus onset is indicated above images. ***B***, Signal time-courses extracted from 0.5 mm concentric rings around the center of the response. The rings are superimposed on images in *A*. On the right panel the initial depolarization for each ring is normalized to 0.1 %. The inset on the right shows the color code. ***C***, Peak depolarization and hyperpolarization (upper panel) and the hyperpolarization ratio (lower panel) as a function of distance from the center.

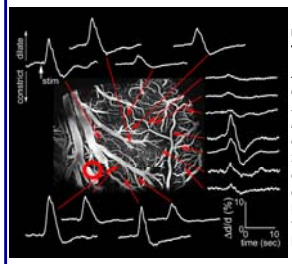

Figure 4. 2-photon laser scanning microscopy measurements of vascular dilation and constriction.

At all locations the initial dilation was followed by a subsequent constriction. The relative strength of dilation and constriction varied as a function of distance from the center of neuronal activity (red circle). White traces show percent diameter change relative to the baseline (Δd/d) at different locations indicated by red arrows.

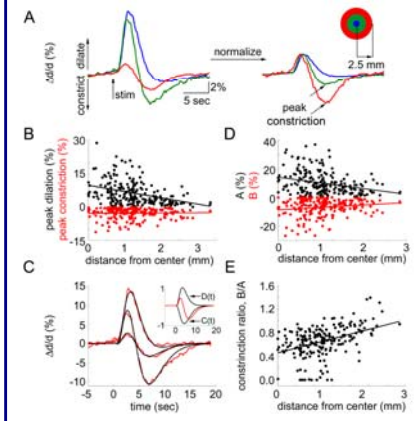

Figure 5. Arteriolar vasodilatation and vasoconstriction as a function of distance from the center of evoked neuronal response.

Good fit to the data assuming a combination of two antagonistic forces support the idea that evoked neuronal excitation is associated with arteriolar vasodilation, while evoked neuronal inhibition is associated with arteriolar vasoconstriction. ***A***, An average of arteriolar diameter changes at 3 concentric distances around the center. ***B***, Peak dilation (upper panel) and peak constriction (lower panel) as a function of distance. Each dot represents a measurement from a single arteriole. ***C***, Three examples of the fit to the data. The inset shows the functions (positive) and (negative) used to fit the data. ***D***, Linear coefficients (upper panel) and (lower panel) as a function of distance. ***E***, The ratio of constriction to dilatation estimated as as a function of distance.

From single vessel to the hemodynamic response: vascular modeling .

We have developed a spatially distributed vascular anatomical network (VAN) model based on microscopically measurable properties to improve quantitative interpretation of the vascular response.

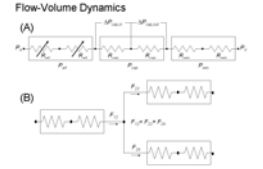

Figure 6. Resistor network representing the vascular network. VAN model is built up from a branching series of individual arterioles, through the capillaries, and then a converging series of venules, each with their own characteristic properties.

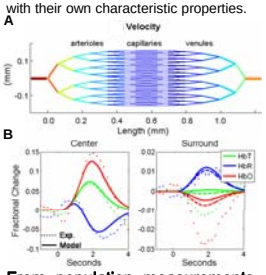

Figure 8. ***A***, 2D vascular network model and the velocity in each segment calculated from the arterial-venial pressure difference and resistance of each vascular segment. The color scale is from 2 mm/s (blue) to 13 mm/s (red). ***B***, The model (solid lines) predicts experimentally measured (dots) changes in hemoglobin concentrations in the center and surround of the rat barrel cortex. The model responses are averaged over the arteriole, capillary, and venule compartments. The dashed lines are the model responses from only the capillary compartment.

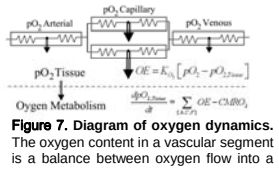

Figure 7. Diagram of oxygen dynamics. The oxygen content in a vascular segment is a balance between oxygen flow into a segment via blood flow and out of the segment via blood flow and oxygen diffusion into the tissue. Hemoglobin oxygenation in each vascular branch is a function of the blood flow, blood volume, and oxygen extraction.

From population measurements of neuronal activity to behavior of identified types of neurons: modeling of neuronal circuits.

- Constraints in present mathematical analysis:

- Mathematical formulation:

$$\phi_{\mathrm{MUA}}(z_j,t_k) = \sum_i M_i(z_j)\, r_i(t_k)$$

$$\phi_{\mathrm{LFP}}(z_j,t_k) = \sum_i L_i(z_j)\,(h * r_i)(t_k)$$

h(t): temporal kernel

From other laminar experiment with less evoked activity:

$h(t) \sim e^{-t/\tau}$

Physiological constraints are explicitly incorporated in the mathematical model: The high-frequency part (multi-unit activity; MUA) is modeled as a sum over contributions from firing activity of multiple cortical populations, while the low-frequency (local field potentials; LFP) is assumed to reflect the dendritic currents due to synaptic inputs evoked by this firing activity.

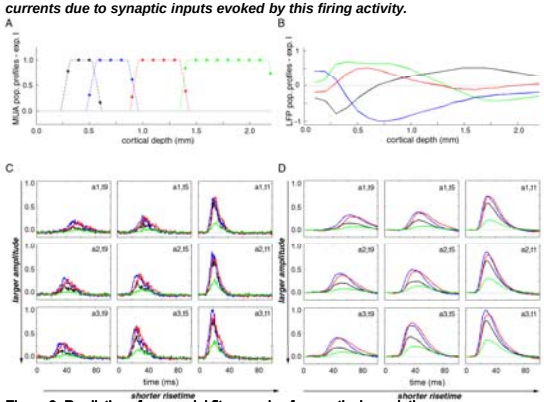

Figure 9. Predictions from model fit assuming four cortical populations.

A, Fitted MUA spatial profiles $M_n(z)$, suggesting the cortical depths of the somata of these populations. ***B***, LFP spatial profiles $L_n(z)$ $(n=1,2,3,4)$ resulting from activity by the efferent synapses of each of these populations. ***C***, Fitted firing rates $r_n(t)$ in the time range 0-100 ms after stimulus onset. ***D***, Fitted synaptic-drive function, i.e., the convolution of the firing rate with the optimised temporal coupling kernel, $(h*r_n)(t)$, in the same time range. ***The model predicts the typical order of firing L4->L2/3->L5->L6***

From optical measurements of hemodynamics to BOLD fMRI.

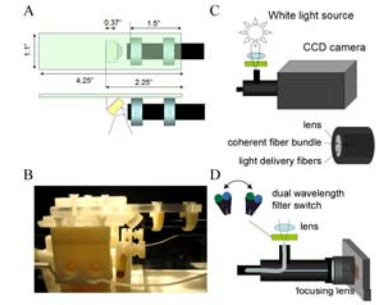

Figure 10. MR-compatible optical imager.

We have developed an MR-compatible optical imager that uses optical fibers to bring illumination light into the bore of the MRI scanner and a high-density coherent fiber bundle (15000 fibers) to transmit the optical signal to a detector, a cooled CCD camera. The imager allows full-field (space-resolved) spectroscopic measurements of Hb, HbO and HbT simultaneously with MRI. Currently we are upgrading the imager to allow fluorescent calcium-sensitive and VSD imaging. ***A***, The distal end of the fiber bundle is coupled to a mirror (yellow). ***B,*** A photograph of the distal end mounted onto the animal holder. ***C-D***, At the proximal end the imaging fibers in the bundle are coupled to a CCD detector. Light from the light source is passed through a dual wavelength filter switch and focused onto illuminating fibers.

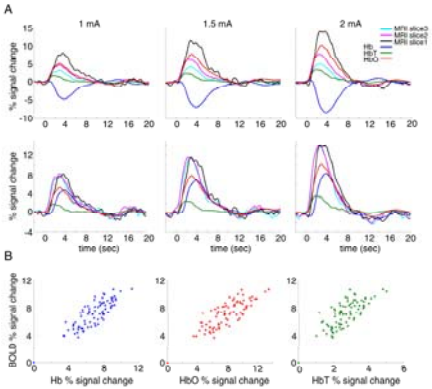

Figure 11. Comparison of functional timecourse of BOLD and optical measures of Hb, HbO and HbT.

BOLD signal from the surface MRI slice had a delayed onset time and a delayed return to the baseline comparing to deeper MRI slices and to the optical measures. This is due to a bias of surface BOLD signal to big draining veins where the signal is delayed comparing to the capillary response. ***A***, Timecourses were extracted from analogous ROIs (~2x2 mm) following spatial coregistration. Three columns correspond to 3 stimulus amplitudes (indicated on top). In the second row BOLD timecourses are normalized to the amplitude of the top slice (slice 1), and Hb is inverted for better visualization of differences in response onset time. 20 trials were averaged for each stimulus condition. ***B***, Trial-to-trail comparison of peak response within the same ROI. Each dot represents one trial. All 3 amplitudes are superimposed.

Co-investigators:

MRI:

Bruce Rosen, Larry Wald, Alex de Crespigny et al.

Optical imaging:

David Boas, Elizabeth Hillman, David Kleinfeld

Vascular modeling: David Boas

Neuronal modeling: Gaute Einevoll et al.

Neurovascular coupling: Anna Devor et al.